American Mineralogist, Volume 79, pages 261–268, 1994

A multinuclear NMR study of synthetic pargasite

Mark D. Welch*
Department of Earth Sciences, University of Cambridge, Downing Street, Cambridge CB2 3EQ, U.K.
Waclaw Kolodziejski, Jacek Klinowski
Department of Chemistry, University of Cambridge, Lensfield Road, Cambridge CB1 1EW, U.K.

Abstract

Atomic order in synthetic end-member pargasite, $NaCa_2{}^{[6]}(Mg_4Al)^{[4]}(Si_6Al_2)O_{22}(OH)_2$, has been examined by high-resolution ^1H, ^{27}Al, and ^{29}Si magic-angle-spinning (MAS) NMR spectroscopy, with and without cross-polarization, and by infrared spectroscopy. The spectra indicate that Al occurs only on T1, M2, and M3 sites and are consistent with 1.5Mg + 0.5Al on M2 and 0.5Mg + 0.5Al on M3, $^{[4]}$Al being ordered onto T1 sites without Al avoidance (Al-O-Al linkages are allowed). Assuming random mixing on sites in these ratios, we calculate a maximum configurational entropy for subordered synthetic pargasite of 38 J/(K·mol). This is much lower than the value of 56 J/(K·mol) indirectly estimated by Westrich and Holloway (1981) from their phase equilibrium study of the low-pressure dehydration of synthetic pargasite. However, we show that it is possible to reconcile their experimental results with our estimate of the configurational entropy. Our results suggest that synthetic pargasite is likely to be a good experimental analogue for natural pargasite.

Introduction

The use of synthetic analogues of natural minerals is a common expedient in experimental mineralogy and petrology. The assumption made is that the behavior of an analogue is essentially representative of its natural counterpart. The chemical and microstructural complexity of natural amphiboles has usually necessitated the use of simplified model synthetic systems in order to reduce the number of intensive variables to be controlled. The system Na_2O-CaO-MgO-Al_2O_3-SiO_2-H_2O (NCMASH) has been used extensively to model the phase relations of petrologically significant natural sodic-calcic amphiboles. A particularly important composition is that of end-member pargasite, $NaCa_2{}^{[6]}(Mg_4Al)^{[4]}(Si_6Al_2)O_{22}(OH)_2$, which has been used as an analogue of high-temperature crustal and upper-mantle amphiboles (e.g., Westrich and Holloway, 1981). Pargasite has space group $C2/m$, and its essential structural features are shown in Figure 1. $C2/m$ amphiboles have two distinct types of tetrahedral site, denoted T1 and T2, and three types of octahedral site, denoted M1, M2, and M3. Two Al and six Si atoms are distributed over the tetrahedral sites, and four Mg atoms and one Al atom over the octahedral sites. Many natural pargasite samples closely approach end-member stoichiometry, with some substitution of Fe^{2+} for Mg and Fe^{3+} for Al. However, it has been recognized that trivalent octahedral cations (most notably Al^{3+} and Fe^{3+}) in natural amphiboles are highly ordered onto the M2 sites, whereas in synthetic analogues, Al^{3+}, Sc^{3+}, and Cr^{3+} are highly disordered over all octahedral sites. On the other hand, Semet (1973) found that Fe^{3+} is significantly ordered onto M2. Raudsepp et al. (1987) used infrared spectroscopy and Rietveld analysis to study a range of synthetic fluor- and hydroxy-pargasite with different trivalent octahedral ions (M^{3+} = Al, Sc, Cr, Ga, and In), and found that the degree of ordering of these ions increases with F content. A similar observation has been made on a binary series of fluor-hydroxy-pargasite (M^{3+} = Al) by McMillan et al. (1985), who found a systematic decrease in the Mg_2Al Raman absorption (corresponding to non-M2$^{[6]}$Al) with increasing F content, suggesting progressive ordering of Al onto M2. Raudsepp et al. measured ^{19}F, ^{27}Al, and ^{29}Si MAS NMR spectra for fluor-scandian-pargasite, $NaCa_2{}^{[6]}(Mg_4Sc)^{[4]}(Si_6Al_2)O_{22}F_2$, and concluded that Al and Si were disordered over T1 and T2 sites with Al avoidance in force. They did not, however, study the site occupancies of end-member hydroxy-pargasite by NMR. Their infrared spectrum suggests that there is some octahedral Mg-Al disorder, though it was not quantified.

We have measured high-resolution ^1H, ^{27}Al, and ^{29}Si MAS NMR spectra (the last two with and without cross-polarization, abbreviated as CP MAS) of synthetic end-member hydroxy-pargasite to determine atomic configurations on octahedral and tetrahedral sites.

Experimental Methods

Sample preparation and characterization

A sample (0.6 g) of end-member hydroxy-pargasite was synthesized at 1 kbar and 930 °C (70 h) from a stoichi-

* Present address: Department of Mineralogy, The Natural History Museum, Cromwell Road, London SW7 5BD, U.K.

0003–004X/94/0304–0261$02.00

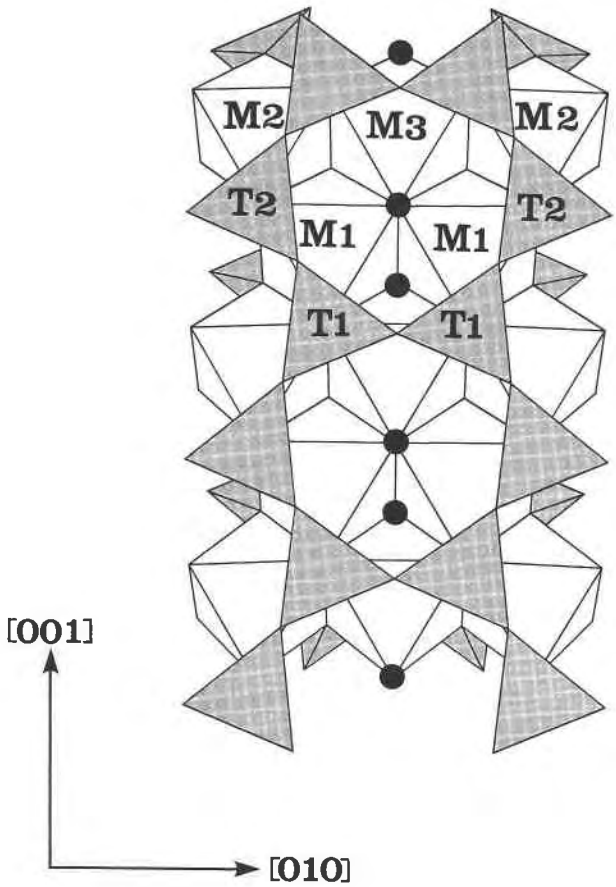

Fig. 1. Octahedral and tetrahedral sites in $C2/m$ amphiboles. OH groups are shown as solid circles. The O-H bond is parallel to $a \sin \beta$ with the H located midway between the planes of apical O (O1, O2) and the T atoms, being approximately equidistant (~3.1 Å) from O1, O2, T1, and T2.

ometric gel prepared by the method of Biggar and O'Hara (1969). Checks on sample purity by optical microscopy, scanning electron microscopy, and powder X-ray diffraction indicate that the product consists of amphibole and small amounts of diopside and possibly nepheline (~5% total). Crushing and reheating this product at 1 kbar and 932 °C for two more days reduced the amounts of impurities to ~2%, but further crushing and heating did not improve the amphibole yield. The final product comprised prismatic cylindrical amphibole crystals up to 45 μm long and 10 μm in diameter. Wavelength-dispersive electron microprobe analysis indicated that, within analytical error, the amphibole has the ideal stoichiometry (Table 1). HRTEM revealed that the amphibole is essentially free of chain multiplicity and chain-arrangement faults. Unit-cell parameters (Table 1) were derived from powder X-ray diffraction using a Guinier camera, Ni-filtered Cu$K\alpha$ radiation, and a Si internal standard.

Magic-angle-spinning NMR

The ^{29}Si, ^{27}Al, and ^{1}H MAS NMR spectra were recorded at 297 K and 79.5, 104.2, and 400.1 MHz, respectively. Zirconia MAS rotors were spun in air. The ^{29}Si spectra were acquired with MAS at 4 kHz using $\pi/3$ pulses and 180-s recycle delays. The Hartmann-Hahn condition for ^{1}H-^{29}Si cross-polarization was set on a sample of kaolinite (Rocha and Klinowski, 1991) and the CP MAS spectrum of pargasite was acquired using single contacts with 5 μs $\pi/2$ pulses on the ^{1}H channel, 8-ms contact times, and 5-s recycle delays. Single-pulse ^{27}Al spectra were measured with MAS at 14.5 kHz using very short, 0.6-μs (<10°), radio-frequency pulses, and 0.5-s recycle delays. The CP MAS spectrum of ^{1}H-^{27}Al was recorded with a single contact, a contact time of 500 ms, a ^{1}H $\pi/2$ pulse of 3.5 μs, a recycle delay of 3 s, and a spinning rate of 5 kHz. The Hartmann-Hahn condition was established in one scan on the kaolinite sample using similar acquisition parameters. As only the central $\frac{1}{2} \leftrightarrow -\frac{1}{2}$ transition is observed, excitation is selective and the Hartmann-Hahn condition is $3\gamma_{Al}B_{Al} = \gamma_{H}B_{H}$, where γ_{Al} and γ_{H} denote the gyromagnetic ratios of ^{27}Al and ^{1}H, and B is the radio-frequency field strength.

Table 1. Chemical and unit-cell data for synthetic pargasite

Oxide	Ideal wt%	Ideal atoms pfu (O = 23)	Average wt% (n = 15)	Average atoms pfu
SiO_2	43.13	6.00	43.18(0.69)	6.02(0.04)
Al_2O_3	18.30	3.00	18.19(0.66)	2.99(0.03)
MgO	19.29	4.00	19.26(0.76)	3.99(0.06)
CaO	13.42	2.00	13.15(0.30)	1.96(0.03)
Na_2O	3.17	1.00	3.91(0.06)	1.06(0.03)
Total	97.85	16.00	97.69(3.83)	16.02(0.19)

Note: a = 9.905(2), b = 17.943(3), c = 5.281(1) Å, β = 105.58(1)°, V = 904.0(3) Å^3. Numbers in parentheses refer to errors in the last decimal place.

Infrared spectroscopy

Infrared spectra were collected using a Fourier-transform infrared spectrometer (Bruker IFS 113V) with a DTGS detector and KBr beam splitter. Spectra were collected in the range 3600–4000 cm^{-1}. All spectra were integrated over 512 scans. Instrumental resolution was 2 cm^{-1}. Powdered samples were dried for 1 h at 130 °C before preparing pellets. Because of the small amount of OH in the samples, it was necessary to use 0.04–0.05 g of powder per pellet to obtain a good signal-to-noise ratio. The powder was interspersed with 0.2 g of KBr matrix material and then dried at 130 °C and stored in a desiccator.

Results

^{29}Si MAS NMR

The ^{29}Si MAS NMR and CP MAS spectra of pargasite are shown in Figure 2. The ^{29}Si MAS NMR spectrum is best simulated (i.e., it gives the smallest residuals) by a five-peak fit with Gaussian peaks at −87.5, −86.1, −84.5, −82.0, and −78.6 ppm, with relative intensities (peak areas) of 21.1, 14.5, 16.5, 38.1, and 9.8%, respectively. A discussion of the possible nature of the broad peak at −87.5 ppm is given in a later section. All peaks cross-

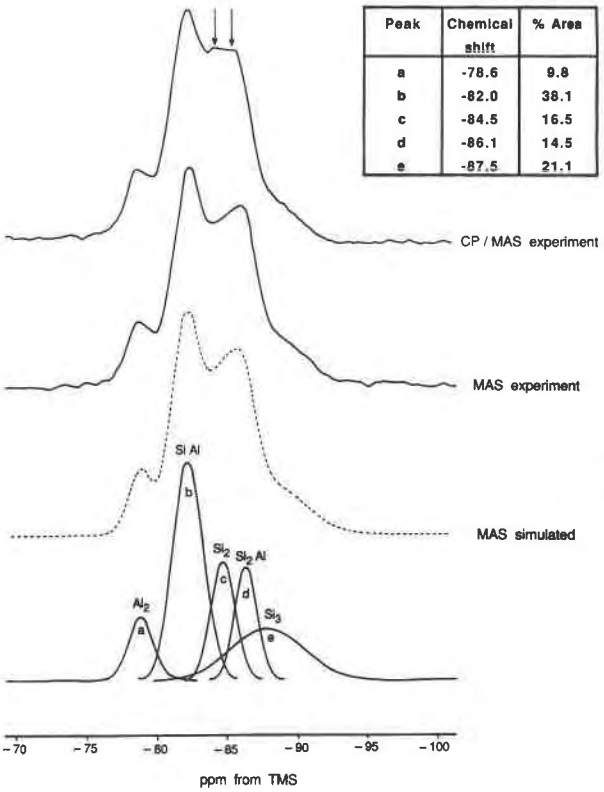

Fig. 2. The ^{29}Si MAS NMR spectra of pargasite. The inset shows the intensity associated with each peak. The CP MAS spectrum clearly resolves the −84.5-ppm peak (c) and the −86.1-ppm peak (d) (marked with arrows).

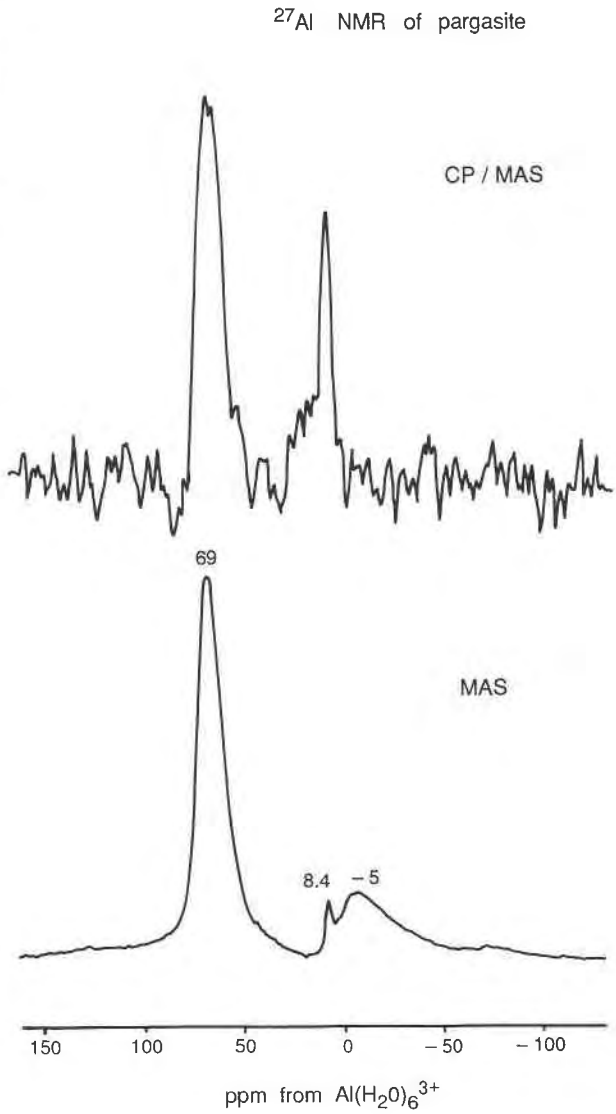

Fig. 3. The ^{27}Al MAS NMR spectra of pargasite. The CP MAS spectrum reveals that only one of the two octahedral peaks (8.4 ppm) cross-polarizes. The other octahedral peak must, therefore, be due to Al on M2 sites. The strong peak at 69 ppm is due to $^{[4]}$Al.

polarize. The CP MAS spectrum indicates that the peaks at −84.5 and −86.1 ppm (marked with arrows) both cross-polarize and so correspond to two distinct peaks. In effect, a four-site simulation combines these two peaks and gives larger residuals. The CP MAS spectrum indicates that this is not justified. The discrepancy cannot be attributed to impurities because the only ones observed were trace amounts (2%) of diopside and, possibly, nepheline. Both are anhydrous and so do not contribute to ^{1}H-^{29}Si cross-polarization. Optical microscopy and SEM did not reveal the presence of any other amorphous or crystalline phases.

^{27}Al MAS NMR

The ^{27}Al MAS NMR and CP MAS spectra of pargasite are shown in Figure 3. The ^{27}Al MAS NMR spectrum contains three peaks at 68.5, 8.4, and −5 ppm. The 68.5 ppm peak is by far the strongest and corresponds to $^{[4]}$Al. The other two peaks are due to $^{[6]}$Al. Again, the $^{[4]}$Al peak cross-polarizes, as expected. The ^{27}Al CP MAS spectrum shows that only resonances due to $^{[4]}$Al and the $^{[6]}$Al peak at 8.4 ppm cross-polarize and so belong to Al sites near protons. Therefore, we provisionally assign the 8.4 ppm resonance to Al on M1 or M3 sites (these are bonded to OH), and −5 ppm resonance to Al on the M2 sites. The $^{[4]}$Al/$^{[6]}$Al peak intensity ratio of 3.5 is much higher than the ideal value of 2.0. However, electron microprobe data (Table 1) indicate a very close approach to ideal pargasite stoichiometry, and the microprobe analytical uncertainties allow a maximum ratio of 2.05. The ^{27}Al MAS NMR results suggest that there are ~2.33 $^{[4]}$Al. Quadrupolar effects associated with ^{27}Al nuclei can complicate the deconvolution of ^{27}Al MAS NMR spectra. One effect is reduced peak intensity, which leads to an underestimate of site occupancies, particularly the octahedral sites that experience larger quadrupole effects than the tetrahedral sites. We can reconcile the ^{27}Al MAS NMR spectrum with the microprobe data, if we assume that ^{27}Al MAS NMR underestimates the total amount of $^{[6]}$Al by 9%.

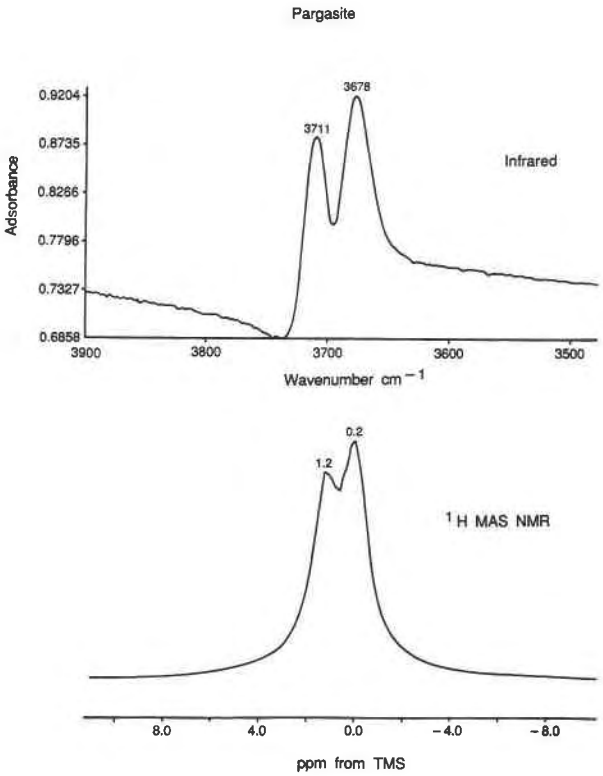

Fig. 4. **(Top)** Infrared and **(bottom)** ^{1}H MAS NMR spectra of pargasite in the OH stretching region. The peaks at 3711 and 3678 cm^{-1} are due to Mg_3-OH and Mg_2Al-OH configurations, respectively. Deconvolution of the NMR spectrum indicates that the peaks are of equal intensity.

^{1}H MAS NMR and infrared spectroscopy

The infrared and ^{1}H MAS NMR spectra of pargasite are shown in Figure 4. The infrared spectrum of pargasite has two peaks of comparable intensity at 3678 and 3711 cm^{-1} and is almost identical to the spectrum published by Raudsepp et al. (1987) who conventionally assigned these peaks to Mg_2Al and Mg_3 octahedral groups bonded to OH, respectively. The ^{1}H MAS NMR spectrum confirms that there are two distinct proton next nearest neighbor environments, corresponding to the resonances at 0.2 and 1.2 ppm. Spectral simulation shows that the peak intensities (areas) are equal.

Although accurate site occupancies cannot be derived from infrared peak intensities, this is possible by ^{1}H MAS NMR spectroscopy, which samples nearest and next nearest neighbor sites. Here, peak intensity is directly proportional to site occupancy. To achieve that it is necessary to consider the intensity contributions made by spinning sidebands associated with each of the nuclear environments. Under the operating conditions used in the ^{1}H MAS NMR experiment (spinning at 4.5 kHz and with a spectral width of 100 kHz), spinning sidebands for the peaks at 0.2 and 1.2 ppm in the ^{1}H MAS NMR spectrum should occur at $\pm$10–13 ppm. For protons, a spectral width of 100 kHz corresponds to $\pm$125 ppm, which would allow the spinning sidebands to be found. However, we found that essentially all peak intensity was located in the two intense peaks. No detectable peak intensity is present in the spinning sidebands.

Discussion

Tetrahedral sites

Four end-member models exist for the interpretation of tetrahedral site occupancies in pargasite. These are summarized in Table 2, which shows the number of ^{27}Al and ^{29}Si peaks predicted for each model. Models 1 and 2 have all Al ordered on T1 sites, with and without Al avoidance, respectively. In models 3 and 4 Al is disordered over all tetrahedral sites, with and without Al avoidance, respectively. Further constraints are placed upon Q^2-Q^3 peak intensity ratios in the ^{29}Si MAS NMR spectrum such that the summed Q^3 contribution to the total spectral peak intensity is 33% for models 1 and 2 and 50% for models 3 and 4 (Raudsepp et al., 1987). Although we indicate the various tetrahedral environments for Al in Table 2, quadrupolar peak broadening is likely to mean that these different tetrahedral configurations are not resolved in the ^{27}Al MAS NMR experiment. Consequently, our interpretation of tetrahedral site occupancies is based upon the ^{29}Si MAS NMR spectra. Given that impurities are essentially absent (traces of diopside and nepheline, but no amorphous or crystalline hydrous phases), the spectrum is interpreted only in terms

Table 2. Models for the tetrahedral site occupancies in pargasite

Model*	No. of peaks			
	^{29}Si	^{27}Al	^{29}Si NNN** environments	^{27}Al NNN† environments
Model 1	4	1	Si_2Al	Si_3
T1 + AA			Si_2 $SiAl$ Al_2	
Model 2	5	2	Si_3 Si_2Al	Si_3 Si_2Al
T1 − AA			Si_2 $SiAl$ Al_2	
Model 3	6	2	Si_2Al $SiAl_2$ Al_3	Si_3 Si_2
T1 + T2 + AA			Si_2 $SiAl$ Al_2	
Model 4	7	7	Si_3 Si_2Al $SiAl_2$ Al_3	Si_3 Si_2Al $SiAl_2$ Al_3
T1 + T2 − AA			Si_2 $SiAl$ Al_2	Si_2 $SiAl$ Al_2

* Model with Al avoidance = +AA, and model without Al avoidance = −AA.
** Next nearest neighbor.
† The number of peaks refers to $^{[4]}$Al.

TABLE 3. Evaluation of models for tetrahedral sites, where subpeaks of −88-ppm peak are all Q^2 or all Q^3

Combination	−88 ppm	−86 ppm	−85 ppm	−82 ppm	−79 ppm	Score %
5A	2	3	2	2	3	25
5B	2	2	3	2	3	27
5C	2	3	3	2	2	31
5D	3	2	2	2	3	31
5E	3	3	2	2	2	36
5F	3	2	3	2	2	38
5G	2	2	2	3	3	48
5H	2	3	2	3	2	53
5I	2	2	3	3	2	55
5J	3	2	2	3	2	59
6A	(33)	2	2	2	3	31
6B	(33)	3	2	2	2	36
6C	(33)	2	3	2	2	38
6D	(22)	3	3	2	3	41
6E	(33)	2	2	3	2	59
6F	(22)	3	2	3	3	63
6G	(22)	2	3	3	3	65
6H	(22)	3	3	3	2	69
7A	(333)	2	2	2	3	31
7B	(333)	3	2	2	2	36
7C	(333)	2	3	2	2	38
7D	(333)	2	2	3	2	59
7E	(222)	3	3	3	3	79

TABLE 4. Evaluation of models for tetrahedral sites, with mixed subpeaks for −88-ppm peak

Combination	−88 ppm	−86 ppm	−85 ppm	−82 ppm	−79 ppm	Score %
6I	(32)	3	3	2	2	31
6J	(32)	3	2	3	2	53
6K	(32)	2	3	3	2	55
6L	(32)	3	2	2	3	25
6M	(32)	2	3	2	3	27
6N	(32)	2	2	3	3	48
7F	(332)	3	3	2	2	31
7G	(332)	3	2	3	2	53
7H	(332)	3	2	2	3	25
7I	(332)	2	3	3	2	55
7J	(332)	2	2	3	3	48
7K	(332)	2	3	2	3	27
7L	(322)	3	3	3	2	69
7M	(322)	3	3	2	3	41
7N	(322)	2	3	3	3	65
7O	(322)	3	3	3	3	79

Note: the score is the percent contribution of the Q^3 intensity to the total spectral intensity, excluding that from the −88-ppm subpeaks.

of pargasite stoichiometry and structure. As we mentioned in the previous section, spectral simulation suggests that a five-peak model (Model 2) is the best. A four-peak model is ruled out by the CP MAS spectrum, which indicates that there are at least five cross-polarizing peaks.

The broadness of the −88-ppm peak deserves special consideration, as it could imply that this peak is composed of several subpeaks. A plausible interpretation of the likely nature of this peak is essential to the choice of occupancy model. Pargasite stoichiometry requires that there are four, five, six, or seven peaks in the ^{29}Si MAS NMR spectrum. Hence, the −88-ppm peak can, at most, be composed of three subpeaks. Using this constraint we can attempt to discriminate between five-, six-, and seven-peak models as follows. Initially, we consider all possible distinct combinations of Q^2 and Q^3 peaks for each of the three models, remembering that the −88-ppm peak is composed of one, two, or three subpeaks in the five-, six-, and seven-peak models, respectively. Having determined the possible combinations, we evaluate each with reference to the observed peak intensities, again remembering that the −88-ppm peak (be it single or composite) contributes 21% of the total spectral intensity. Values for the total Q^3 (or Q^2) contribution to each possible spectrum indicate how plausible a five-, six-, or seven-peak model is in each case. The constraints imposed upon spectrum selection are as follows.

1. There should be two, three, and four Q^3 peaks in the five-, six-, and seven-peak models, respectively. All three models have three Q^2 peaks.

2. In the six- and seven-peak models, the Q^3 contribution to the −88-ppm peak is equal to the ideal model value of 50% minus the sum of the Q^3 contributions to the other peaks.

3. The six-peak spectral simulation requires the −88-ppm peak to consist of two subpeaks with equal areas; the seven-peak spectral simulation requires that the three subpeaks composing the −88-ppm peak have approximately equal areas.

4. The high-to-low field Q sequence should be plausible in the light of known dependencies of ^{29}Si chemical shifts with the degree of Si condensation and the number of next nearest neighbor Al. This is discussed in detail later in this section.

The complete set of all possible combinations for five-, six-, and seven-peak models is shown in Tables 3 and 4. Clearly, the multiplicity of each combination for 6I–6N is two and for 7F–7O is three. In Table 4, combinations with scores above 50% imply that the −88-ppm subpeaks are all Q^2. Although combinations such as 6J, 6K, and 7G only just require this, others with scores much higher than 50% (7L, 7N, and 7O) are highly implausible. Some combinations in Table 4 score just under 50% (e.g., 6N, 7J), implying a very small (2%) Q^2 contribution to the −88-ppm peak. Conversely, scores such as 25–31% (6I, 6L, and 6M and 7F, 7H, and 7K) imply that essentially all of the −88-ppm peak must be Q^3 to reach the required score of 50%. This leads to violations of the first constraint. We estimate from the experimental error of ±1% on each peak area that the tolerances on the ideal scores for the three models are about ±5%. This corresponds to acceptable scores of 28–38% for the five-peak model and 45–55% for the six- and seven-peak models.

If one bears the foregoing comments in mind, Tables 3 and 4 indicate that combinations 5A–5F, 6I, and 6L, and 7F, 7H, 7J, 7K, and 7M are possible choices. The tolerances on six- and seven-peak scores (ideal fit = 45–55%) allow unlikely combinations involving very small (<3%) contributions from Q^2 or Q^3 subpeaks. Constraint 3 excludes 6I, and 6L on the grounds that it implies that the areas of the two subpeaks are very unequal. For similar reasons, combinations 7F, 7H, 7J, 7K, and 7M are improbable.

TABLE 5. Compilation of pyribole ^{29}Si chemical shifts

Phase	Si_3	Si_2	Reference
Tremolite	−91	−88	Smith et al. (1983)
Tremolite	−90	−87	Raudsepp et al. (1987)
Sodian magnesiocummingtonite	−90, −88	−85, −84	Welch et al. (1992)
Sodian jimthompsonite	−92	−88, −86	Welch et al. (1992)
Fluor-scandian-pargasite*	−90	−83	Raudsepp et al. (1987)
Enstatite		−84, −81	Smith et al. (1983)
Diopside		−85	Smith et al. (1983)

* Calculated from Rietveld refinement data.

A further qualitative constraint (no. 4 above) upon the choice of combinations is provided by consideration of the high-to-low field Q sequences in the light of existing data on ^{29}Si chemical shifts for pyriboles, (Smith et al., 1983; Raudsepp et al., 1987; Welch et al., 1992). Table 5 is a compilation of these data and indicates that in pyriboles Si_3 occurs at fields 3–8 ppm higher than where Si_2 occurs in all cases. This strongly suggests that combinations in which the −88-ppm peak comprises only Q^2 subpeaks should be rejected. Smith et al. (1983) compiled ^{29}Si chemical shifts for Q^4 environments in framework silicates and found that chemical shifts were displaced systematically down field as the number of Al next nearest neighbors increased. The high-to-low field sequence is Si_4, Si_3Al, Si_2Al_2, $SiAl_3$, Al_3. The ^{29}Si chemical shifts have also been predicted from calculations using T-O-T bond angle and ⟨T-O⟩ bond length data. Raudsepp et al. (1987) calculated ^{29}Si chemical shifts of different Q^2 and Q^3 configurations for fluor-scandian-pargasite using crystallographic data obtained by Rietveld refinement. Their calculated high-to-low field sequence is Si_3, Si_2Al, $SiAl_2$, Si_2, Al_3, $SiAl$, Al_2. The chemical shifts for Si_2 and $SiAl_2$ are almost identical, suggesting that they could be transposed in other aluminous amphiboles, i.e., Si_3, Si_2Al, Si_2, $SiAl_2$, Al_3, $SiAl$, Al_2. Only combination 5E satisfies all the above constraints, and so this five-peak model is preferred. The peaks in the ^{29}Si MAS NMR spectrum of Figure 2 are labeled to accord with this choice. Hence, we suggest that all $^{[4]}Al$ is located on T1 sites without Al avoidance operating.

Octahedral sites

The OH stretching frequency in amphiboles is very sensitive to the occupancy of the M1 and M3 sites, and so these sites can be studied by infrared spectroscopy. In amphiboles the correlation between OH stretching frequency and the occupancies of M1 and M3 sites is well known (e.g., Ernst and Wai, 1970; Raudsepp et al., 1987). We mentioned above that ^1H MAS NMR can be used to quantify proton populations, provided that account is taken of the contributions from spinning sidebands. We have found that all the measured spectral intensity is contained in the two peaks at 0.2 and 1.2 ppm and that their peak intensities are equal.

In order to explore Mg and Al site occupancies on M1, M2, and M3 sites in pargasite, we consider seven models for the interpretation of the infrared and ^1H MAS NMR spectra. These are shown in Table 6. The configuration assignments are based upon the known frequency dependencies in amphibole infrared spectra, as mentioned previously. The probabilities correlate directly with expected peak intensity ratios in ^1H MAS NMR spectra and are calculated for random mixing on sites. The low probabilities of the $MgAl_2$ configuration for four- and five-site models are well within the detection limits of ^1H MAS NMR and infrared spectroscopy and are clearly absent. All models other than 3b can be rejected on the grounds that they predict the wrong number of peaks in the spectra. Consequently, we are left with 3b as the most acceptable model. However, this model predicts a peak intensity ratio of 2:1. The observed 1:1 ratio of Mg_3 and Mg_2Al peak intensities is consistent with there being 1.5Mg + 0.5Al on M2 and 0.5Mg + 0.5Al on M3. The deviation from model 3b arises simply because Mg and Al are not randomly distributed over all three sites. There may, however, be random mixing of Mg and Al within M2 and M3 sites.

COMPARISONS WITH PREVIOUS STUDIES OF PARGASITE

The maximum configurational entropy allowed by the spectroscopic data is calculated as follows. S_{cfg} (pargasite) $= S_{cfg}[M2] + S_{cfg}[M3] + S_{cfg}[T1] = -2R(0.75 \ln 0.75 + 0.25 \ln 0.25) - R \ln 0.5 - 4R \ln 0.5 = 9.35 + 5.76 + 23.05 = 38.16$ J/(K·mol). This is considerably less than the value for pargasite [~56 J/(K·mol)] indirectly estimated by Westrich and Holloway (1981) from the low-pressure subsolidus dehydration of synthetic pargasite. The question arises, are the spectroscopic data for subordered pargasite reconcilable with the experimental bracket estimate of Westrich and Holloway? In the absence of heat capacity data for pargasite, a rigorous comparison cannot be attempted. However, if we assume that the raw experimental data of Westrich and Holloway and their derived values for ΔH_r^0 and ΔS_r^0 are accurate, and we make the assumption that ΔC_P for the reaction is zero (as they had to), we can attempt a reconciliation. We assume that the values of $\Delta H_r^0 = 328.3$ kJ/mol and $\Delta S_r^0 = 170.6$ J/(K·mol) are correct. With no enthalpy data for pargasite we can only address the entropy, i.e., we assume that the ordering enthalpy is negligible. A source of configurational entropy not considered by Westrich and Hollo-

way is Mg-Al mixing in partially inverted $MgAl_2O_4$ spinel. Wood et al. (1986) have shown that at temperatures of 900–1050 °C $MgAl_2O_4$ is 40% inverted. Westrich and Holloway synthesized their spinel at 1500 °C, and so the initial degree of inversion could have been rather higher. If we take it that the spinels in the phase equilibrium products had reequilibrated to ~40% inversion, then 7 J/K of configurational entropy is added to ΔS_r^0. Carpenter (1991) has shown that anorthite synthesized from glass is highly Al-Si disordered. However, when it is then annealed at 1400 °C for 1 h, it has the $I\bar{1}$ Al-Si ordered structure. This suggests that the anorthite synthesized by Westrich and Holloway at 1500 °C for 72 h and then annealed at 1300 °C for 48 h is likely to be essentially Al-Si ordered and, because of stoichiometry and strict Al avoidance, does not contribute to configurational entropy.

The Westrich and Holloway model (1981) for the configurational entropy of synthetic pargasite has the following characteristics: (1) random mixing of Al and Si on all tetrahedral sites, (2) random mixing of Mg and Al on M2 sites, and (3) random mixing of Na and vacancies on two A sites, A2 and Am. In order to evaluate the entropy Westrich and Holloway used the site occupancies of Al refined by Robinson et al. (1973) for several natural pargasite samples for which the average Al content of the tetrahedral sites is 0.40 and 0.09 for T1 and T2, respectively, and where $^{[6]}$Al occurs only on M2 sites. This leads to a configurational entropy of 55.9 J/(K·mol). The maximum possible configurational entropy for end-member pargasite (random mixing of Al and Si on all tetrahedral sites, Mg and Al on all octahedral sites, and Na and vacancies on a split A site) is 69.7 J/(K·mol).

In calculating the configurational entropy of pargasite and comparing it with the model of Westrich and Holloway, we must also consider a possible contribution from a split A site. For amphiboles with full A sites, the maximum contribution from mixing on A2 and Am sites is 11.5 J/(K·mol), an appreciable amount. Evidence for or against a split A site can be obtained from infrared spectroscopy. For example, Robert et al. (1989) studied the evolution of the OH stretching absorption at 3714–3735 cm^{-1} for Na···OH configurations in sodian and potassian richterite as a function of F substitution. For fluor-hydroxy sodian richterite they observed that progressive fluorination causes splitting of the peak at 3730 cm^{-1} into two (separated by 5 cm^{-1}) and a shift to higher frequency. In their spectrum of the hydroxy end-member this peak is not split. Robert et al. presented a convincing argument for the splitting of the peak being due to a split A site. In our infrared spectrum of pargasite (Fig. 4), the corresponding peak occurs at 3711 cm^{-1} and is not split. From this we infer that the A site in synthetic pargasite is not split and therefore does not contribute to configurational entropy.

The approach we use is to take the nonconfigurational entropy of reaction, calculated using values for third-law entropies for the products and pargasite, and then add to ΔS_r^0 the difference between fully disordered and subordered pargasite [56 − 38 = 18 J/(K·mol)] and also the 7 J/K from partially inverse spinel. Values for the third-law entropies of the product phases were taken from Holland and Powell (1990). The value of 582 J/(K·mol) for pargasite is taken from Holland (1989) as the best available estimate in the absence of heat capacity data. From this we calculate a nonconfigurational ΔS_r^0 = 149 J/K. Hence, the total ΔS_r^0 = 149 + 18 + 7 = 174 J/K. This value is in good agreement with the 171 ± 6 J/K obtained by Westrich and Holloway. This treatment suggests that it is possible to reconcile the phase equilibrium data with a subordered pargasite.

TABLE 6. Probabilities of configurations of atoms bonded to OH in pargasite*

Model	Sites	Mg_3OH	Mg_2AlOH	$MgAl_2OH$	Al_3OH
1 site	M3	0.00	1.00	0.00	0.00
2 site (a)	M1	0.25	0.50	0.25	0.00
2 site (b)	M2	1.00	0.00	0.00	0.00
3 site (a)	M1 + M3	0.30	0.44	0.22	0.04
3 site (b)	M2 + M3	0.67	0.33	0.00	0.00
4 site	M1 + M2	0.56	0.38	0.06	0.00
5 site	all	0.51	0.38	0.10	0.01

* The calculation assumes random mixing on sites.

In his review of amphibole crystal chemistry, Hawthorne (1981) concluded that there is no direct evidence of Al occupying M1, M3, or T2 sites in natural amphiboles. The question of whether or not Al-avoidance operates in natural amphiboles is still open. Our results are consistent with the ordering of Al onto T1 sites but also indicate that an appreciable amount of Al occurs on M3 as well as M2.

ACKNOWLEDGMENTS

M.D.W. acknowledges the support of a University of Cambridge Fellowship and a NERC Special Fellowship. We thank Susan Circone and an anonymous referee for constructive reviews that led to significant improvements in this paper.

REFERENCES CITED

Biggar, G.M., and O'Hara, M.J. (1969) A comparison of gel and glass starting materials for phase equilibrium studies. Mineralogical Magazine, 37, 198–205.

Carpenter, M.A. (1991) Mechanisms and kinetics of Al-Si ordering in anorthite: Incommensurate domain coarsening. American Mineralogist, 76, 1110–1119.

Ernst, W.G., and Wai, C.M. (1970) Infrared, X-ray and optical study of cation ordering and dehydrogenation in natural and heat-treated sodic amphiboles. American Mineralogist, 55, 1226–1258.

Hawthorne, F.C. (1981) Crystal chemistry of the amphiboles. In Mineralogical Society of America Reviews in Mineralogy, 9A, 1–95.

Holland, T.J.B. (1989) Dependence on entropy on volume for silicate and oxide minerals: A review and a predictive model. American Mineralogist, 74, 5–13.

Holland, T.J.B., and Powell, R. (1990) An enlarged and updated internally consistent thermodynamic dataset with uncertainties and correlations: The system K_2O-Na_2O-CaO-MgO-MnO-FeO-Fe_2O_3-Al_2O_3-TiO_2-SiO_2-C-H-O_2. Journal of Metamorphic Geology, 8, 89–124.

McMillan, P.F., Graham, C.M., and Ross, N.L. (1985) Vibrational spectroscopy of F-OH pargasites (abs.). Eos, 66 (18), 309.

Raudsepp, M., Turnock, A., Hawthorne, F.C., Sherriff, B.L., and Hartman, J.S. (1987) Characterization of synthetic pargasitic amphiboles

($NaCa_2Mg_4M^{3+}Si_6Al_2O_{22}(OH,F)_2$; M^{3+} = Al, Cr, Ga, Sc, In) by infrared spectroscopy, Rietveld structure refinement, and ^{27}Al, ^{29}Si and ^{19}F MAS NMR spectroscopy. American Mineralogist, 72, 580–593.

Robert, J.-L., Della Ventura, G., and Thauvin, J.-L. (1989) The infrared OH-stretching region of synthetic richterites in the system Na_2O-K_2O-CaO-MgO-SiO_2-H_2O-HF. European Journal of Mineralogy, 1, 203–211.

Robinson, K., Gibbs, G.V., Ribbe, P.H., and Hall, M.R. (1973) Cation distributions in three hornblendes. American Journal of Science, 273A, 522–535.

Rocha, J., and Klinowski, J. (1991) Kaolinite as a convenient standard for setting the Hartmann-Hahn Match for ^{29}Si CP/MAS NMR of silicates. Journal of Magnetic Resonance, 90, 567–568.

Semet, M. (1973) A crystal-chemical study of synthetic magnesiohastingsite. American Mineralogist, 58, 480–494.

Smith, K.A., Kirkpatrick, R.J., Oldfield, E., and Henderson, D.M. (1983) High-resolution silicon-29 nuclear magnetic resonance spectroscopic study of rock-forming silicates. American Mineralogist, 68, 1206–1215.

Welch, M.D., Rocha, J., and Klinowski, J. (1992) Characterization of polysomatism in biopyriboles: Double-/triple-chain lamellar intergrowths. Physics and Chemistry of Minerals, 18, 460–468.

Westrich, H.R., and Holloway, J.R. (1981) Experimental dehydration of pargasite and calculation of its entropy and Gibbs energy. American Journal of Science, 281, 922–934.

Wood, B.J., Kirkpatrick, R.J., and Montez, B. (1986) Order-disorder phenomena in $MgAl_2O_4$ spinel. American Mineralogist, 71, 999–1006.

Manuscript received April 9, 1993
Manuscript accepted November 22, 1993